Films of directionally oriented carbon nanotubes as counter electrodes for electrochromic devices

Mehdi Costalin, Issam Mjejri, Nicolas Penin, Oudomsack Viraphong, Vesselin Shanov, Aline Rougier

Films of directionally oriented carbon nanotubes as counter electrodes for electrochromic devices

Mehdi Costalin[1], Issam Mjejri[1], Nicolas Penin[1], Oudomsack Viraphong[1], Vesselin Shanov[2], Aline Rougier[1*]

[1]CNRS, Univ. Bordeaux, Bordeaux INP, ICMCB, UMR 5026, F-33600 Pessac, France

[2]Dept of Chemical and Environmental Engineering, University of Cincinnati, Cincinnati, OH 45221, USA

*Corresponding Author: aline.rougier@icmcb.cnrs.fr, ICMCB-CNRS, 87 avenue du Dr Albert Schweitzer, 33608 Pessac cedex, France

Keywords: CNT films, Counter electrode, Electrochromic devices

ABSTRACT: Connected displays are the salient nature of our e-connected society requiring high-quality electronic conductive materials integrated in smart devices. Herein, we highlight the use of carbon nanotubes (CNTs) not only as substitutes for ITO (In_2O_3:Sn) but mainly as a counter electrode for electrochromic devices (ECDs). Using a dry spinning process, conductive CNT films with directionally oriented tubes were successfully laid on polyethylene terephthalate (PET) flexible substrates. The CNTs were synthesized as vertically aligned spinnable arrays by chemical vapor deposition. The transparency and optical absorption properties were tuned by adjusting the number of CNT layers (L) within the film from light gray for 1L to dark black above 10L. The CNT films, showing pseudo-capacitive to capacitive behavior in lithium-based electrolytes, were further integrated in ECDs based on poly(3,4-ethylenedioxythiophene) polystyrene sulfonate (PEDOT:PSS) active layers. The fabricated PET/ITO/PEDOT:PSS/electrolyte/CNT/PET device exhibited reproducible and clear color switching from light to dark blue with a coloration efficiency of 88 $cm^2 \cdot C^{-1}$. This study highlights novel architecture of ECDs using CNT-based films as conductive counter electrode.

1. Introduction

Electrochromic devices (ECDs) able to modulate their optical properties under an applied voltage find applications in several domains [1–3]. Apart from smart windows for energy efficiency of buildings, which are mostly based on oxides and particularly WO_3 that switches from a transparent to a blue state upon reduction [4–6], electronic displays represent an

emerging field combining high demand and huge challenges [7,8]. To address this need, adjustment of both the materials and the appropriate device architecture is required. Often described as an optical battery, five-type-layer ECDs are based on the transparent conductive oxide (TCO)/EC1/electrolyte/EC2/TCO chain, in which EC1 and EC2 correspond to electrochromic layers. The performance of the ECDs, specifically for the switching kinetics, relies on the TCO layers, among which the most popular is ITO (In_2O_3:Sn). Considering sustainable aspects [9], intensive research has been devoted to the replacement of ITO by other oxides, such as FTO (SnO_2:F), ZnO, or other materials including Ag nanowires and graphene. Herein, special attention is focused on the benefit of carbon nanotubes (CNTs) having in mind the necessity to be either transparent for transmissive displays or opaque for reflective displays while simultaneously maintaining a high electrical conductivity. Indeed, thanks to their outstanding mechanical and conductive properties, CNTs can challenge the brittle ITO.

Following research interest of more than 20 years, CNTs are now promising active players in various fields including thermoelectric research [10], electronic chemical sensors [11], and ECDs [12]. In ECDs, the use of CNTs has been mostly illustrated on one hand through electrochromic properties of CNT films integrated in all CNT ECDs [13–15], and on the other hand through their mixture with electrochromic materials aiming at increasing their electronic conductivity [16,17]. In this work, we introduce a novel approach using CNTs as a counter electrode in a four-layer device configuration, schematized by the ITO/EC/electrolyte/CNT chain [18]. Additionally, we specifically investigated the application of dry spun thin films of CNTs, allowing to cover a range of transparent to opaque films [19,20].

Since the discovery of the electronic-conductivity properties of polyacetylene, conductive polymers have been highly regarded in the organic semiconductor field. In addition, their emission and reflection properties make them good candidates for electro-emissive devices. Compared with inorganic electrochromic materials, organic electrochromic materials reveal advantages such as a broader color palette, higher coloration efficiency, and greater optical contrast [21–23]. Recent studies have demonstrated the suitability of many techniques, including spray coating, ink jet, and doctor blading, for deposition of thin films of conducting polymers with good control of the process. Indeed, the choice of the processing method not only affects the energy required to activate the devices, but also their stability. In terms of materials, most commercially available inks are poly(3,4-ethylenedioxythiophene) (PEDOT)-based. Exploring the feasibility of transferring lab-scale prototypes to commercial products, we recently developed PEDOT-based devices [18,24]. These devices offer change in color from colorless or light blue to dark blue depending on film thickness. In this paper, we went a step

forward in building original EC devices by combining CNTs as the counter electrode to a PEDOT-based active layer.

2. Experimental

2.1. Synthesis of drawable CNT arrays and CNT film integration

The CNT sheet fabrication starts with synthesis of CNTs using the chemical vapor deposition process [25,26]. The CNTs are grown as vertical arrays on silicon substrates using the patented catalyst and synthesis process. These arrays can then be drawn out into sheets owing to their unique spinnability property. The narrow range of gas flow parameters and catalyst specifications were perfected over the course of years to give very consistent production of spinnable CNT arrays. The dry drawn layers have very high purity and thickness of about 100 nm [26]. A fine control of the number of CNT layers (L) allows building displays covering various optical properties from transparent to opaque. A polyethylene terephthalate (PET) film was placed on the drums on which the CNT layers were collected. In order to densify the formed CNT film with different number of layers, acetone carried by Ar through a two-channel nozzle was sprayed on it immediately after drawing. The two-channel nozzle is part of a small B-290 commercial atomizer made by Buchi. This instrument allows atomization of the feed in the carrier gas and enables formation of droplets with diameter range of 1–25 μm, when employing a tip with 0.7-mm diameter. Illustration of the CNT film formation and the home-made setup used, controlled by a computer, is shown in **Fig. 1**. The morphology of the layers was investigated using a JEOL JSM-840 (operating at 15 kV) scanning electron microscope (SEM JEOL JSM-840, JEOL SAV-Europe, Croissy sur Seine, France). X-ray diffraction (XRD) was performed on a Philips PW 1820, PANalytical X'Pert instrument, 2θ range of 10–80° and $\lambda_{CuK\alpha1}$ = 1.54056 Å.

2.2. Electrochromic ink formulation and film deposition

The electrochromic inks were formulated from commercial, poly(3,4-ethylenedioxythiophene) polystyrene sulfonate, PEDOT:PSS ink (Agfa Orgacon EL-P5015), here called PEDOT:PSS paste. This high-viscosity commercial paste (>100,000 mPa·s), made for screen printing, was first homogenized with a three-roll mill and then diluted with ethanol to lower the viscosity as follows. For the PEDOT:PSS ink, a mixing ratio of 40 wt % of PEDOT:PSS paste and 60 wt % of ethanol was prepared. The resulting dilute solution was stirred for 15 min at room temperature, then dispersed using an ultrasonic bath for 15 min and stirred again for 15 min.

The PEDOT:PSS films were deposited with a bar coater (K control from RK PrintCoat Instruments, Erichsen RK controle, Valence, France) onto ITO-PET substrates (commercialized by SOLEMS with a resistance of 90 $\Omega \cdot \square^{-1}$ and ITO thickness of 90 nm), then dried at 120 °C for 5 min on a hot plate. From an earlier study, an optimization of the color contrast was reported for an 880-nm PEDOT:PSS film deposited using a 40-µm bar (referred as bar n°4) film [24]. This condition was used in the current study.

2.3. Display fabrication

All displays were built in an asymmetric configuration, using PEDOT:PSS/ITO/PET as the working electrochromic electrode and PET/CNT as the counter electrode. Both electrodes were separated by an electrolytic membrane consisting of a commercial lithium-ionic-liquid-based solution of lithium bis(trifluoromethanesulfonyl)imide in 1-ethyl-3-methylimidazolium bis(trifluoromethanesulfonyl)imide (EmimTFSI:LiTFSI (9:1 Molar Ratio, Solvionic, 99.9 %) blended with 40 wt % of poly(methyl methacrylate) (PMMA) dissolved in butanone. Powder of TiO_2 (titanium (IV) oxide ≥99% Sigma Aldrich, Merck KGaA, Darmstadt, Germany) was added as a white opaque pigment in weight ratio of 90/10. The resulting mixture was stirred for 15 min at room temperature, then dispersed using an ultrasonic bath for 15 min and stirred again for 15 min. The electrolyte mixture was then deposited by bar coating (bar n°8, wet thickness 100 µm) on the PEDOT:PSS/ITO/PET electrode. After 30 s of butanone evaporation, both the counter electrode and the electrolyte/PEDOT:PSS/ITO/PET electrode were assembled and pressed manually for a final display configuration PET/ITO/PEDOT:PSS/(EmimTFSI:LiTFSI + PMMA + TiO_2)/CNT/PET. Displays of 2.5 cm × 1.5 cm were built.

2.4. Electrochromic measurements

Electrochemical measurements of CNT thin films on PET were carried out in a three-electrode cell configuration using a BioLogic SP50 potentiostat/galvanostat apparatus (BioLogic SP50, Seyssinet Pariset, France). The counter and reference electrodes consisted of a platinum foil and saturated calomel electrode (SCE; E_{SCE} = 0.234 V/NHE), respectively. The operating voltage was controlled between −1.0 and +1.0 V at a scan rate of 20 $mV \cdot s^{-1}$, in lithium-based electrolyte: lithium bis-trifluoromethanesulfonimide (LiTFSI, Solvionic, purity N 99.99%) in 1-ethyl-3-methylimidazoliumbis(trifluoromethanesulfonyl)-imide (EMITFSI, purity N 99.99%). All electrochemical measurements were performed at room temperature. The optical transmittance of CNT thin films was measured *in situ* using a Varian Cary 5000 UV−VIS−NIR spectrophotometer.

Regarding the displays, the electrochemical analysis was performed in a two-electrode configuration, using a BioLogic SP50 potentiostat/galvanostat apparatus. Colorimetry analysis was carried out using a Konica Minolta CM-700D spectrophotometer with SCE 10°/D65 configuration (Konica Minolta Sensing Europe B.V., Roissy, France), allowing direct determination of colorimetric parameters of the International Commission on Illumination (CIE) L*a*b* color space.

3. Results and discussion

3.1. CNT film properties

The properties of the CNT layers and films are pre-determined by the carbon nanotubes incorporated in them. The synthesized CNTs within the spinnable arrays are about 350 μm long, with diameter of 10–12 nm and 2–6 walls. More details about their characterization can be found in [19,26,27]. The visual appearance of the CNT layers is shown in **Fig. 2** as a function of the number of layers. The higher the numbers of paths, the thicker is the layer and the darker it appears, from light gray to dark black. Above 10 L, all layers are deep black. The XRD pattern of the 10-layer CNT is mainly characterized by an intense peak located at 25.83°, characteristic of a graphitic structure (002) **(Fig. 3)** [27].

Detail of the CNT sheet under SEM at different magnifications is shown in **Fig. 4**, showing the directional alignment of the CNT bundles. Details about the CNT sheet morphology including the tubes themselves were observed using TEM at different magnifications (**Fig. 5**). These images allow clear observation of the directional orientation of individual CNTs along their length.

The visual appearance of CNT films deposited on PET substrate for 1–10 layers (i.e. 1L–10L) as well as the optical transmittance recorded at 250–3000 nm is shown in **Fig. 6**. The transmittance spectrum of commercial ITO on PET is added for comparison. The transmittance spectra of the CNT films above 10L is not included because all CNT films have a dark black appearance above 10L. Simultaneously, the transmittance rapidly decreases as the number of paths increases. However, for 1L and 2L CNTs, it remains higher than that for PET-ITO above 1250 nm, suggesting interesting properties in the near infra-red. The cycling properties of CNT films in three-electrode cells are presented in **Fig. 7**. The overall rectangular shape of the Cyclic Voltammogram CV (**Fig. 7**), in agreement with literature [28–31], typically describes a capacitive to pseudo-capacitive behavior for CNT-based electrodes. The increase in the number of CNT layers is associated with an increase in capacity from 3.5 to 14.8 $mC \cdot cm^{-2}$ for 5L to 50

L, of which evolution remains non-linear. The multiplication of the number of layers by 10 corresponds to an increase of capacity of 4.2, suggesting that as the number of the CNT layers increases, the overall proportion of the active electrochemical surface decreases. This increase of capacity with CNT electrode thickness has been demonstrated in previous work on glassy electrodes [30]. The corresponding chronoamperograms (**Fig. 8**) illustrate fast kinetics upon oxidation/reduction increasing within a few seconds with the number of CNT layers, and a good stability upon cycling with a well-reversible process.

3.2. CNT-based ECDs

The CNT films were successfully integrated in full devices using PEDOT:PSS as active electrochromic layers. The electrochemical performance of the PEDOT:PSS/electrolyte/CNT displays built using various numbers of CNT layers (1L, 5L, and 20L) are shown in **Fig. 9a**. The rectangular-like shape of the CV is typical of an overall pseudo-capacitive behavior. The stability and reversibility are satisfactory upon cycling, even for the device with one CNT layer. Governed by the electrochromic behavior of the PEDOT:PSS layer, the device switches from a light blue to a dark blue state (**Fig. 9b**). The optical contrast was evaluated using the CIE L*a*b* color system. In the CIE colorimetric space, the color is represented by three parameters – a luminance axis (L*) and two hue axes (a*) and (b*) – which can be used to define and quantitatively compare the colors. The optical contrast ΔE* is defined by equation (1):

$$\Delta E^* = [(L^*_c - L^*_b)^2 + (a^*_c - a^*_b)^2 + (b^*_c - b^*_b)^2]^{1/2} \quad (1)$$

The determination of the chromaticity parameters show a modulation of L*, a*, and b*, from 49.62, −3.55, and −7.78 in the oxidized state, respectively, to 40.79, −1.76, and −14.06 in the reduced state, leading to ΔE* of 9.73.

The well-pronounced reversibility is confirmed for corresponding chronoamperometry measurements performed at +1.0 and −1.5 V/60 s, showing a symmetrical response in both oxidation and reduction steps (**Fig. 9c**). The capacity of the device increases stepwise with the number of CNT layers showing values of 1.1, 1.8, and 2.4 $mC \cdot cm^{-2}$ for CNT of 1L, 5L, and 20L, respectively. In comparison with the single layers, the capacity of the device remains lower suggesting a limitation from the PEDOT layers associated with the use of a solid electrolyte membrane. Indeed, the full device configuration implies interfaces in between the various layers of which quality appears to be thickness dependent. Due to poor adhesion between the electrolyte and the CNT-50L layer, all attempts at building ECDs associating CNT-50L and

PEDOT:PSS films were unsuccessful. Additionally, ion mobility might be hindered in the thick CNT-50L counter electrode.

The corresponding diffuse reflectance for the oxidized (+1.0 V) and reduced (−1.5 V) states are shown in **Fig. 9d**. A value of ΔR of 13% is reached, associated with a color modulation from light to deep blue (**Fig. 9d**). In addition to the reflectance modulation ΔR, coloration efficiency (CE) is one of the key parameters to be taken into account when aiming at applications. The CE is defined as the change in optical density (OD) per unit charge density (Q) and can be calculated using equation (2):

$$CE = \Delta OD/Q \qquad (2)$$

where $\Delta OD = \log(R_{oxi}/R_{red})$, Q is the electronic charge injected into the electrochromic material per unit area, R_{oxi} is the reflectance in the oxidized state, and R_{red} is the reflectance in the reduced state. A CE of 88 $cm^2\ C^{-1}$ is obtained. Interestingly, this value is higher than that reported for ECDs in similar four-layer configuration using an Ag layer as the counter electrode (i.e. ECD_{Ag}, CE = 69 $cm^2 \cdot C^{-1}$ [24]) showing the key role that CNTs could play as counter electrodes for novel ECDs in the field of displays.

4. Conclusion

Herein, using a dry spinning process, transparent-gray to opaque black CNT films were successfully deposited and used as substitutes of the ITO layer and counter electrodes in ECDs. The PEDOT:PSS/electrolyte/CNT device exhibited reproducible and clear color switching from light blue to dark blue with CE of 88 $cm^2 \cdot C^{-1}$. Further improvement of EC performance using CNT counter electrodes is in progress by adding metallic particles on top of the CNTs. This work opens new directions for ECDs with original architecture that allow addressing a large panel of optical modulation.

■ AUTHOR INFORMATION

Corresponding Author

*E-mail: aline.rougier@icmcb.cnrs.fr.

ORCID

Aline ROUGIER: 0000-0002-1340-734X

Issam MJEJRI: 0000-0001-5313-3198

CRediT author statement

Mehdi Costalin: Conceptualization, Deposition, Characterization, original draft preparation. **Issam Mjejri:** Conceptualization, Deposition, Characterization. **Oudomsack Viraphong:** Conceptualization, Deposition, Characterization. **Nicolas Penin**: Conceptualization, Deposition, Characterization. **Vesselin Shanov:** Supervision, Writing, Reviewing. **Aline Rougier:** Supervision, Writing, Reviewing.

NOTES

The authors declare no competing financial interest.

■ ACKNOWLEDGMENTS

One of the co-authors (Vesselin Shanov) would like to acknowledge the financial support of NASA through Grant # NNC16CA17C.

■ ABBREVIATIONS

LiTFSI, lithium trifluoromethanesulfonimide; EMITFSI, 1-ethyl-3-methylimidazolium bis(trifluoromethanesulfonyl)imide; PEDOT:PSS, poly(3,4-ethylenedioxythiophene) polystyrene sulfonate

■ DATA AVAILABILITY STATEMENT

The raw/processed data required to reproduce these findings cannot be shared at this time due to technical or time limitations.

References

[1] C.G. Granqvist, M.A. Arvizu, I.B. Pehlivan, H.-Y. Qu, R.T. Wen, G.A. Niklasson, Electrochromic materials and devices for energy efficiency and human comfort in buildings: a critical review, Electrochim. Acta. 259 (2018) 1170–1182. https://doi.org/10.1016/j.electacta.2017.11.169.

[2] N. Miura, M. Nishimura, H. Urano, Organic electrochromism for a new color electronic paper, Sol. Energy Mater. Sol. Cells. 92 (2008) 136–139. DOI:10.1016/j.solmat.2007.02.027.

[3] E.L. Runnerstrom, A. Llordés, S.D, Lounis, D.J. Milliron, Nanostructured electrochromic smart windows: traditional materials and NIR-selective plasmonic nanocrystals, Chem. Comm. 50 (2014) 10555–10572. DOI: 10.1039/c4cc03109a.

[4] M. Da Rocha, Y. He, X. Diao, A. Rougier, Influence of cycling temperature on the electrochromic properties of WO_3//NiO devices built with various thicknesses, Sol. Energy Mater. Sol. Cells. 177 (2018) 57–65. https://doi.org/10.1016/j.solmat.2017.05.070.

[5] D. Ma , T. Li, , Z. Xu, L. Wang, J. Wang, Electrochromic devices based on tungsten oxide films with honeycomb-like nanostructures and nanoribbons array, Sol. Energy Mater. Sol. Cells. 177 (2018) 51–56. https://doi.org/10.1016/j.solmat.2017.06.009.

[6] S.C. Nunes, S. M. Saraiva, R.F.P. Pereira, S. Pereira, M.M. Silva, L.D. Carlos, E. Fortunato, R.A.S. Ferreira, R. Rego, V.Z. Bermudez, Sustainable dual-mode smart windows for energy efficient buildings, ACS Appl. Energy Mater. 2 (2019) 1951–1960. DOI: 10.1021/acsaem.8b02041.

[7] L. Gomes, A. Branco, T. Moreira, F. Feliciano, C. Pinheiro, C. Costa, Increasing the electrical conductivity of electrochromic PEDOT-PSS films. A comparative study, Sol. Energy Mater. Sol. Cells. 144 (2016) 631–640.
https://ds.doi.org./10.1016/j.solmat.2015.10.001.

[8] B. Schmatz, A.W. Lang, J.R. Reynolds, Fully printed organic electrochemical transistors from green solvents, Adv. Funct. Mater. 29 (2019) 1905266.
DOI: 10.1002/adfm.201905266.

[9] U. Posset, M. Harsch, A. Rougier, B. Herbig, G. Schottner, G. Sextl, Environmental assessment of electrically controlled variable light transmittance devices, RSC Adv. 2 (2012) 5990–5996. https://doi.org/10.1039/C2RA20148H.

[10] T. Fujigaya, Development of thermoelectric conversion materials using carbon nanotube sheets, Bull. Chem. Soc. Jpn. 92 (2019) 400–408. doi:10.1246/bcsj.20180272.

[11] V. Schroeder, S. Savagatrup, M. He, S. Lin, T.M. Swager, Carbon nanotube chemical sensors, Chem. Rev. 119 (2019) 599−663. DOI: 10.1021/acs.chemrev.8b00340.

[12] K. Yanagi, R. Moriya, Y. Yomogida, T. Takenobu, Y. Naitoh, T. Ishida, H. Kataura, K. Matsuda, Y. Maniwa, Electrochromic carbon electrodes: controllable visible color changes in metallic single-wall carbon nanotubes, Adv. Mater. 23 (2011) 2811–2814. DOI: 10.1002/adma.201100549.

[13] M.L.Moser, G. Li, M. Chen, E. Bekyarova, M.E. Itkis, R.C. Haddon, Fast electrochromic device based on single-walled carbon nanotube thin films, Nano Lett. 16 (2016) 5386−5393, 80 (2016) 480–486. DOI: 10.1021/acs.nanolett.6b01564.

[14] D. Stekovic, B. Arkook, G. Li, W. Li, E. Bekyarova, M.E. Itkis, High modulation speed, depth, and coloration efficiency of carbon nanotube thin film electrochromic device achieved by counter electrode impedance matching, Adv. Mater. Interfaces. 5 (2018) 1800861. DOI: 10.1002/admi.201800861.

[15] F.J. Berger, T.M. Higgins, M. Rother, A. Graf, Y. Zakharko, S. Allard, M. Matthiesen, J.M. Gotthardt, U. Scherf, J. Zaumseil, From broadband to electrochromic notch filters with printed monochiral carbon nanotubes, ACS Applied Mater Interf. 10 (2018) 11135−11142. DOI: 10.1021/acsami.8b00643.

[16] S. Liu, W. Wang, Improved electrochromic performances of WO_3-based thin films via addition of CNTs, J. Sol Gel Sci. Technol. 80 (2016) 480–486. DOI:10.1007/s10971-016-4093-1.

[17] K. Xu, Q. Zhang, Z. Hao, Y. Tang, H. Wang, J. Liu, H. Yan, Integrated electrochromic supercapacitors with visual energy levels boosted by coating onto carbon nanotube conductive networks, Sol. Energy Mater. Sol. Cells. 206 (2020) 110330. https://doi.org/10.1016/j.solmat.2019.110330.

[18] A. Danine, L. Manceriu, C. Faure, C. Labrugère, N. Penin, A. Delattre, G. Eymin-Petot-Tourtollet, A. Rougier, Toward simplified electrochromic devices using silver as counter electrode material, ACS Applied Mater Interf. 11 (2019) 34030–34038. https://doi.org/10.1021/acsami.9b12380.

[19] V. Shanov, W. Cho, R. Malik, N. Alvarez, M. Haase, B. Ruff, N. Kienzle, T. Ochmann, D. Mast, M. Schulz, CVD growth, characterization and applications of carbon nanostructured materials, Surf. Coat. Technol. 230 (2013) 77–86. https://doi.org/10.1016/j.surfcoat.2013.06.017.

[20] T. Wang, D. Zhao, N. Alvarez, V. Shanov, B. Heineman, Optically transparent carbon nanotube film electrode for thin layer spectro-electrochemistry, Anal. Chem. 87 (2015) 9687–9695. https://doi.org/10.1021/acs.analchem.5b01784.

[21] R.J. Mortimer, D.R. Rosseinsky, P.M.S. Monk (Eds.) Electrochromic Materials and Devices, Wiley-VCH, Weinheim, Germany, 2015.

[22] S. Hassab, E.D. Schen, A.M. Osterholm, M. Da Rocha, G. Song, Y. Alesanco, A. Vinuales, A. Rougier, J.R. Reynolds, J. Padilla, A new standard method to calculate electrochromic switching time, Sol. Energy Mater. Sol. Cells. 185 (2018) 54–60. https://doi.org/10.1016/j.solmat.2018.04.031.

[23] W.-N. Wu, H.-F. Yu, M.-H. Yeh, K.-C. Ho, Incorporating electrospun nanofibers of TEMPO-grafted PVDF-HFP polymer matrix in viologen-based electrochromic devices, Sol. Energy Mater. Sol. Cells. 185 (2020) 54–60. DOI: 10.1016/j.solmat.2019.110375.

[24] D. Levasseur, I. Mjejri, T. Rolland, A. Rougier, Color tuning by oxide addition in PEDOT:PSS-based electrochromic devices, Polymers. 11 (2019) 179. https://doi.org/10.3390/polym11010179.

[25] V. Shanov, M. Schulz, Methods of growing carbon nanotubes and forming a carbon nanotube thread, US Patent 9,796,121 B2, October 24, 2017.

[26] N. Alvarez, P. Miller, M. Haase, N. Kienzle, L. Zhang, M. Schulz, V. Shanov, Carbon nanotube assembly at near-industrial natural-fiber spinning rates, Carbon. 86 (2015) 350–357. https://doi.org/10.1016/j.carbon.2015.01.058.

[27] S. Gbordzoe, S. Yarmolenko, Y.-Y. Hsieh, P.K. Adusei, N.T. Alvarez, S. Fialkova, V. Shanov, Three-dimensional texture analysis of aligned carbon nanotube structures, Carbon 121 (2017) 591–601. https://doi.org/10.1016/j.carbon.2017.06.028.

[28] Y. Zhou, P. Jin, Y. Zhou, Y. Zhu, High-performance symmetric supercapacitors based on carbon nanotube/graphite nanofiber nanocomposites, Sci. Rep. 8 (2018) 9005. DOI:10.1038/s41598-018-27460-8.

[29] J. Trigueiro, R. Lavall, G. Silva, Nanocomposites of graphene nanosheets/multiwalled carbon nanotubes as electrodes for in-plane supercapacitors, Electrochim. Acta. 187 (2016) 312–322. DOI: 10.1016/j.electacta.2015.11.053.

[30] C.V.V.M. Gopi, R. Vinodh, S. Sambasivam, I.M. Obaidat, H.K. Kim, Recent progress of advanced energy storage materials for flexible and wearable supercapacitor: from design and development to applications, J. Energy Storage. 27 (2020) 101035. DOI: 10.1016/ j.est.2019.101035.

[31] X. Jian, H. Li, S. H. Li, Y. Li, Y. Shang, Flexible and freestanding MoS_2/rGO/CNT hybrid fibers for high-capacity all-solid supercapacitors, Carbon. 172 (2021) 132–137. DOI: 10.1016/j.carbon.2020.09.095.

Figures

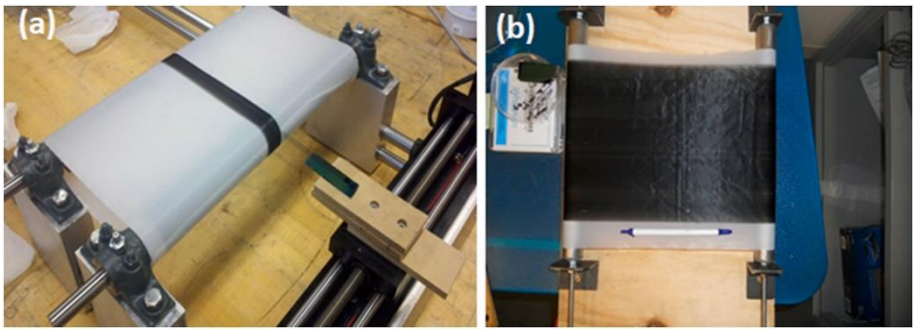

Fig. 1. (a) Home-made setup for dry spinning process of CNT arrays to form one-layer film accumulated on a rotating Teflon belt. The spinnable CNT array grown on a Si substrate is placed on a movable platform thus allowing to cover the entire area of the Teflon belt with CNT film. (b) Picture of CNT film consisted of multiple layers resting on the Teflon belt.

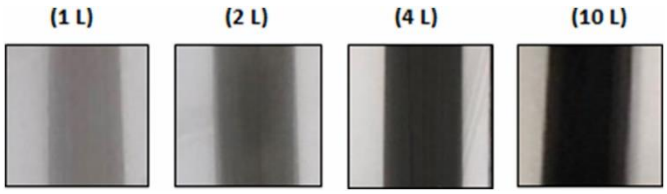

Fig. 2. Visual appearance of CNT films with different layers (1L, 2L, 4L and 10L).

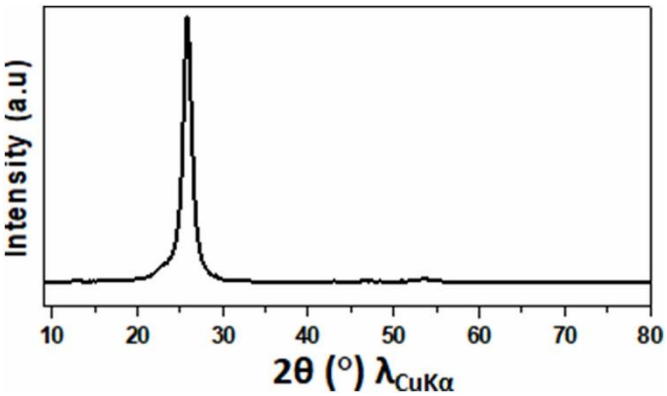

Fig. 3. X-ray diffraction pattern of the CNT 10 L.

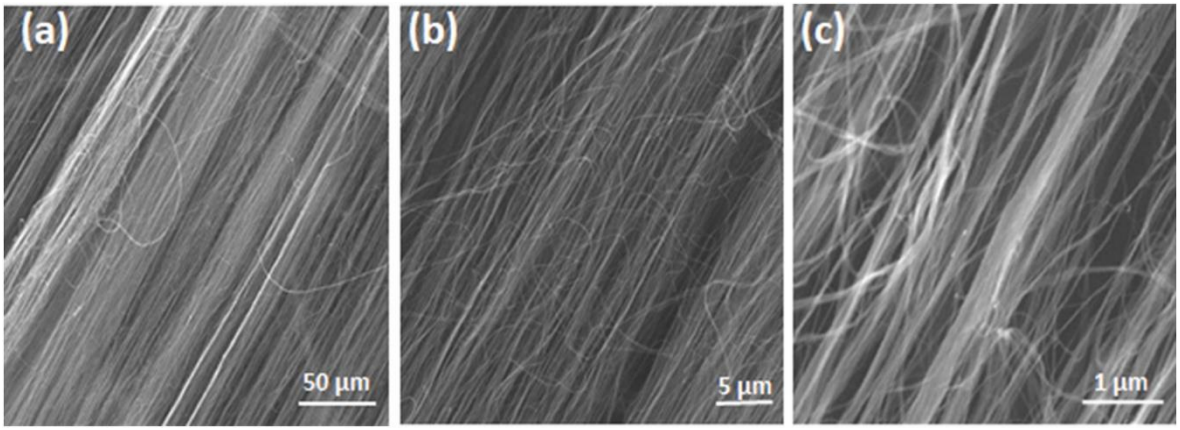

Fig. 4. SEM images of multilayer CNT sheet. Magnification increases from (a) to (c).

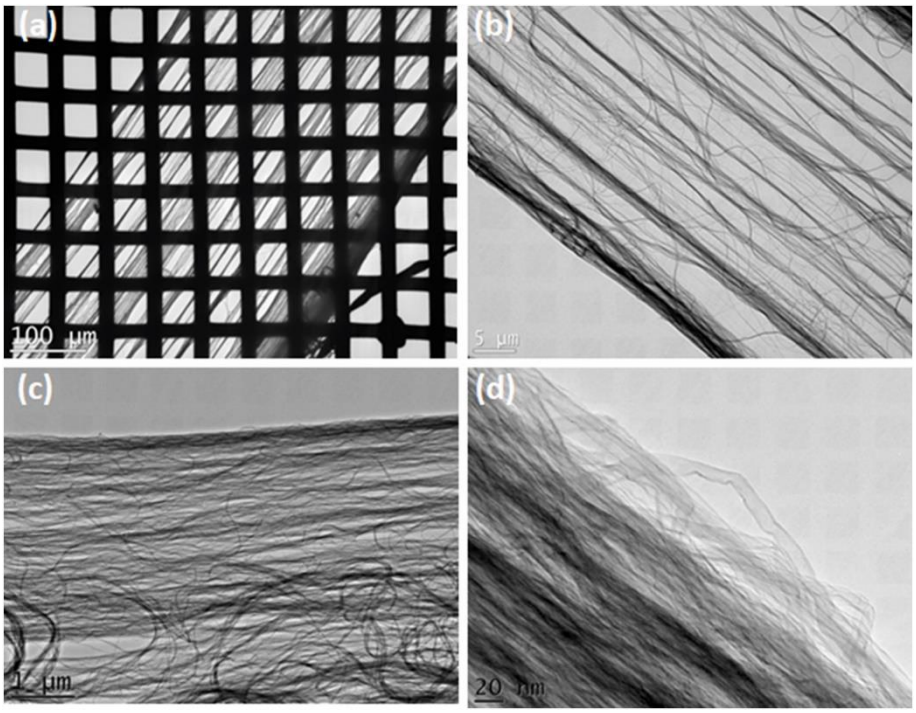

Fig. 5. TEM Images of CNT sheet (ribbon) at different magnifications. Magnification increases from (a) to (d).

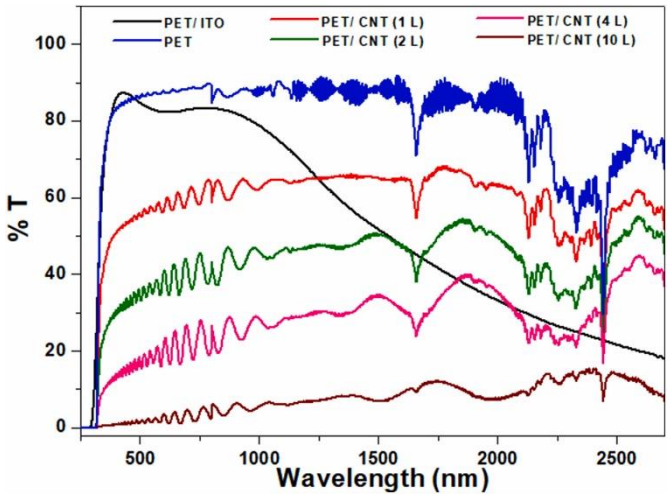

Fig. 6. Optical transmittance spectra of the PET/ITO and PET/CNT with different layers (1L, 2L, 4L and 10L).

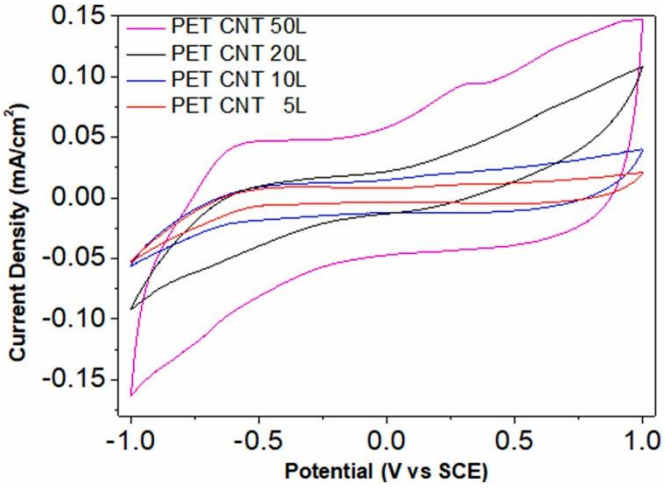

Fig. 7. Cyclic voltammograms of the PET/CNT (5L, 10L, 20L and 50L) in LiTFSI-EMITFSI between −1.0 V and 1.0 V with a 20 mV s^{-1} scan rate.

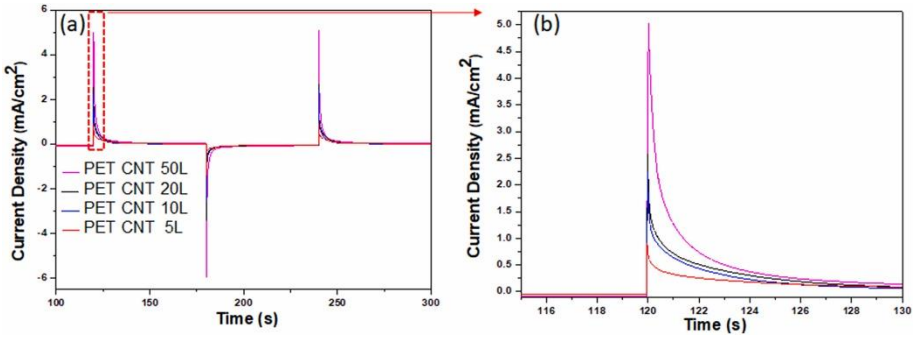

Fig. 8. (a) Chronoamperograms (CA) of the PET/CNT (5L, 10L, 20L and 50L) in LiTFSI-EMITFSI. Potentials of +1.0 V and −1.0 V were applied for 60 s alternatively. (b) Magnification of the 119–125 s region.

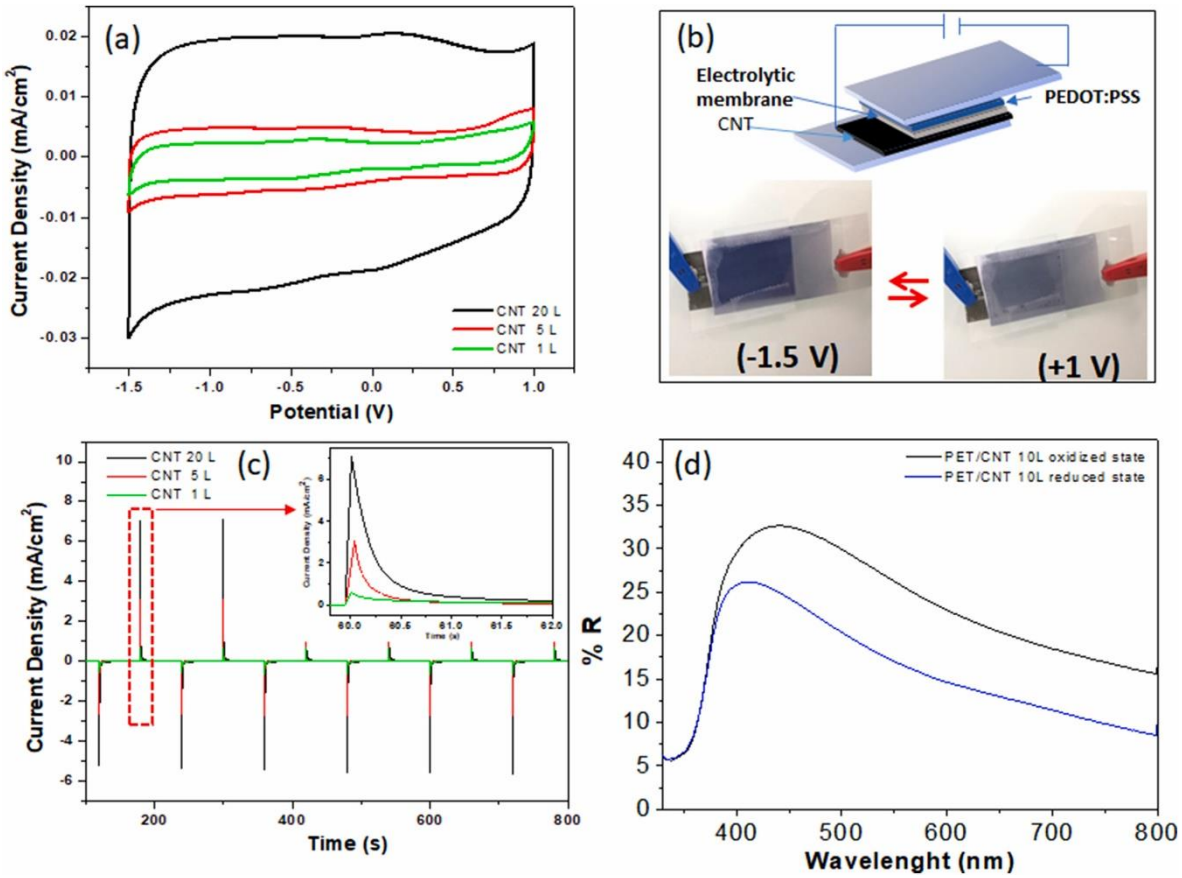

Fig. 9. (a) Cyclic voltammograms of the electrochromic displays (2.5 *1.5 cm^2) built from CNT with varying layers from 1L to 20L. (b) Schematic and visual appearance of EC device in the reduced and oxidized states. (c) chronoamperograms (CA) of the PET/ITO/PEDOT:PSS/LiTFSI-EMITFSI + PMMA + TiO_2/CNT(5L, 20L and 50L/PET. Potentials of +1 V and −1.5 V were applied for 60 s alternatively. (d) *In-situ* optical reflectance spectra at oxidized and reduced states of the electrochromic displays PET/ITO/PEDOT:PSS/LiTFSI-EMITFSI + PMMA + TiO_2/CNT(10L)/PET.